Applied Catalysis B: Environmental 87 (2009) 230–238

Contents lists available at ScienceDirect

Applied Catalysis B: Environmental

journal homepage: www.elsevier.com/locate/apcatb

# Utilization of carbon dioxide as soft oxidant for oxydehydrogenation of ethylbenzene to styrene over $V_2O_5$–$CeO_2$/$TiO_2$–$ZrO_2$ catalyst

Benjaram M. Reddy [a,b], Seung-Cheol Lee [a], Dae-Soo Han [a], Sang-Eon Park [a,*]

[a] Laboratory of Nano-Green Catalysis, Department of Chemistry, Inha University, 253 Yonghyun-dong, Incheon 402-751, Republic of Korea
[b] Inorganic and Physical Chemistry Division, Indian Institute of Chemical Technology, Hyderabad 500007, India

ARTICLE INFO

*Article history:*
Received 4 June 2008
Received in revised form 9 July 2008
Accepted 27 August 2008
Available online 3 September 2008

*Keywords:*
Carbon dioxide
Oxidative dehydrogenation
Ethylbenzene
Styrene
Vanadium oxide
Cerium oxide
Titania–zirconia
Catalyst characterization

ABSTRACT

Vanadium oxide and cerium oxide doped titania–zirconia mixed oxides were explored for oxidative dehydrogenation of ethylbenzene to styrene utilizing carbon dioxide as a soft oxidant. The investigated $TiO_2$–$ZrO_2$ mixed oxide support with high specific surface area (207 $m^2\,g^{-1}$) was synthesized by a coprecipitation method. Over the calcined support (550 °C), a monolayer equivalent (15 wt.%) of $V_2O_5$, $CeO_2$ or a combination of both were deposited by using wet-impregnation or co-impregnation methods to make the $V_2O_5$/$TiO_2$–$ZrO_2$, $CeO_2$/$TiO_2$–$ZrO_2$ and $V_2O_5$–$CeO_2$/$TiO_2$–$ZrO_2$ combination catalysts, respectively. These catalysts were characterized using X-ray diffraction (XRD), Raman, scanning electron microscopy (SEM), transmission electron microscopy (TEM), temperature preprogrammed reduction (TPR), $CO_2$ temperature preprogrammed desorption (TPD) and BET surface area methods. All characterization studies revealed that the deposited promoter oxides are in a highly dispersed form over the support, and the combined acid–base and redox properties of the catalysts play a major role in this reaction. The $V_2O_5$–$CeO_2$/$TiO_2$–$ZrO_2$ catalyst exhibited a better conversion and product selectivity than other combinations. In particular, the addition of $CeO_2$ to $V_2O_5$/$TiO_2$–$ZrO_2$ prevented catalyst deactivation and helped to maintain a high and stable catalytic activity.



## 1. Introduction

Exploitation of carbon dioxide as a soft oxidant for the commercially significant catalytic oxidative dehydrogenation (ODH) of ethylbenzene (EB) to styrene has received enormous interest recently owing to its several attractive features [1–4]. Styrene is one of the most important basic chemicals in the modern petrochemical industry [5,6]. Styrene is normally synthesized by two methods: mainly by an endothermic dehydrogenation of EB and as a co-product of propylene oxide production [5–9]. The ODH of EB is a third possibility to produce styrene employing different oxidants that gained much attention because it can be operated at a lower temperature, as it is exothermic [3,4,10–13]. The dissociation of $CO_2$ on the surface of an appropriate catalyst system produces an active oxygen species, which can take part in the ODH and related reactions [14,15]. Utilization of $CO_2$ in the ODH process, for example, can encompass several advantages such as acceleration of the reaction rate, alleviation of the chemical equilibrium and the enhancement of product selectivity [2].

As per recent studies, various catalyst systems based on mostly Fe-, Cr- or V-oxides exhibited good catalytic activity for the ODH of EB with $CO_2$ as the oxidant [2–4,8,16–23]. Interestingly, various supported vanadium oxide catalysts that are active and selective for selective oxidation, ammoxidation and selective catalytic reduction have also been reported to show better performance for the ODH of EB with $CO_2$ [19,21,23–27]. Contrary to the conventional ODH reaction that uses oxygen, a strong oxidant, the ODH of EB with $CO_2$ has been reported to exhibit much higher selectivity towards styrene. However, the $CO_2$ as an oxidant in the ODH reaction is generally believed to result in the formation of more carbonaceous deposits resulting in the fast deactivation of catalysts. Therefore, there is a need to design better catalyst systems, which can overcome the deactivation.

Although the reaction mechanism of selective oxidation or ODH is not established completely, it is widely believed that breaking of C–H bond in the hydrocarbon is the rate determining step [28], and the reaction proceeds via a Mars-Van Krevelen (redox)-type mechanism [28,29]. Further, it is generally agreed that hydrocarbon oxidation over metal oxide catalysts involves the participation of lattice oxygen species or oxygen vacancies [28,30]. Ceria is a well-known oxygen storage/release capacity (OSC) material widely employed in auto exhaust purification

* Corresponding author. Tel.: +82 32 860 7675; fax: +82 32 872 8670.
*E-mail address:* separk@inha.ac.kr (S.-E. Park).

0926-3373/$ – see front matter © 2008 Elsevier B.V. All rights reserved.
doi:10.1016/j.apcatb.2008.08.026

three-way catalysts (TWC) owing to its high concentration of oxygen vacancies and oxygen-ion mobility character [31]. The $CeO_2$ containing catalysts were also reported to display good catalytic properties for oxidative conversion of propane to propylene and ethane to ethylene, and known to suppress catalyst deactivation by preventing coke formation [32,33]. Therefore, the unique combination of excellent OSC features of $CeO_2$ and oxidizing ability of $V_2O_5$ were thought to result in a good catalyst system for the title reaction. However, bulk $V_2O_5$ and $CeO_2$ are known to suffer from poor thermal stability, mechanical strength and rapid deactivation, and promote nonselective oxidations [34]. Therefore, an appropriate metal oxide support is essential to overcome those deficiencies. The combined titania–zirconia mixed oxides have attracted considerable attention recently as active catalysts as well as supports for a wide variety of reactions [35]. The significant features of $TiO_2$–$ZrO_2$ mixed oxides include a high specific surface area, profound acid–base and redox properties, a high thermal stability and strong mechanical strength [35]. The $TiO_2$–$ZrO_2$ mixed also exhibited a good catalytic activity and selectivity for the ODH of EB with $CO_2$ [36,37]. Therefore, a combination catalyst consisting of $V_2O_5$ and $CeO_2$ over the $TiO_2$–$ZrO_2$ support was undertaken for systematic investigation.

In this study, the $TiO_2$–$ZrO_2$ support was synthesized through a soft-chemical route by adopting a coprecipitation method, and a theoretical monolayer equivalent of $V_2O_5$, $CeO_2$ and combination of both were deposited by a wet impregnation method. The structural evolution of the prepared $TiO_2$–$ZrO_2$, $V_2O_5$/$TiO_2$–$ZrO_2$, $CeO_2$/$TiO_2$–$ZrO_2$ and $V_2O_5$–$CeO_2$/$TiO_2$–$ZrO_2$ combination catalysts was done using X-ray diffraction (XRD), Raman spectroscopy (RS), scanning electron microscopy (SEM), transmission electron microscopy (TEM), temperature preprogrammed reduction (TPR), temperature preprogrammed desorption (TPD), BET surface area and pore size distribution methods. The catalytic performance was evaluated for the ODH of EB to styrene in the vapour phase under normal atmospheric pressure employing $CO_2$ as the soft oxidant.

## 2. Experimental

### 2.1. Catalyst preparation

The $TiO_2$–$ZrO_2$ (1:1 mole ratio) mixed oxide was synthesized by a coprecipitation method from $TiCl_4$ and $ZrOCl_2$ aqueous solutions by hydrolysis with ammonium hydroxide. In a typical experiment, the required quantities of zirconyl(IV) nitrate hydrate (Acros Organics, USA) and titanium(IV) chloride (Yakuri Pure Chemicals, Japan) were dissolved separately in deionized water and mixed together. To this mixture solution, dilute aqueous ammonia (DC Chemicals, Korea) was added drop wise with vigorous stirring until the precipitation was complete (pH 7–8). The resultant precipitates were aged hydrothermally for 12 h at 100 °C before filtration. The well-formed white precipitates were separated by filtration under reduced pressure and washed with deionized water until free from anion impurities. The obtained cake was oven dried at 120 °C for 12 h and finally calcined at 550 °C for 6 h in air atmosphere. On the calcined $TiO_2$–$ZrO_2$ mixed oxide support, a monolayer equivalent of $V_2O_5$ (15 wt.%), $CeO_2$ (15 wt.%) and $CeO_2$–$V_2O_5$ (7.5 wt.% + 7.5 wt.%) were deposited by adopting a standard wet impregnation method. To achieve this, the desired quantities of ammonium metavanadate (Aldrich) and ceric ammonium nitrate (TCI, Japan) were dissolved separately in deionized water to which the finely powdered support was added with continuous stirring. The excess water was evaporated on a water-bath under vigorous stirring. The resulting material was oven dried at 120 °C for 12 h and subsequently calcined at 550 °C for 6 h in air atmosphere. Some portions of the finished samples were again heated at 750 °C for 6 h to investigate their temperature stability. The rate of heating as well as cooling was always maintained at 5 °C $min^{-1}$.

### 2.2. Catalyst characterization

The BET surface area and BJH pore size distribution measurements were made by $N_2$ adsorption/desorption at liquid-nitrogen temperature using a Micromeritics ASAP 2020 instrument. Before analysis, samples were evacuated for 3–4 h at 250 °C in the degassing port of the instrument. Powder XRD patterns were obtained on a Rigaku Multiflex instrument using nickel-filtered Cu Kα (0.15418 nm) radiation source and a scintillation counter detector. The intensity data were collected over a $2\theta$ range of 2–80° with a 0.02° step size and using a counting time of 1 s per point. Crystalline phases were identified by comparison with the reference data from International Center for Diffraction Data (ICDD) files. The Raman spectra were recorded with a LabRam HR800UV Raman spectrometer (Horiba Jobin-Yvon) equipped with a confocal microscope and liquid-nitrogen cooled CCD detector at ambient temperature and pressure. The emission line at 325 nm from He–Cd laser (Melles Griot Laser) was focused on the sample under microscope. The time of acquisition was adjusted according to the intensity of Raman scattering. The SEM images were collected with a JEOL 630-F microscope. Before measurements, samples were dispersed on a steel plate surface and coated with Pt metal. The TEM images were obtained on a JEM-2010 (JEOL) instrument equipped with a slow-scan CCD camera and at an accelerating voltage of 200 kV. Samples were sonically dispersed in ethanol and deposited on a carbon coated copper grid before examination.

The TPR and TPD measurements were made on a Pulse Chemisorb 2705 (Micromeritics, USA) instrument. Before the TPR measurements, the sample was preconditioned by passing dry air (20 ml/min) at 400 °C for 2 h next the temperature was brought down to 100 °C. The TPR was run from 100 to 700 °C at a heating rate of 10 °C/min in 5% $H_2$ and argon gas mixture. For TPD measurements, a high purity $CO_2$ was adsorbed at 100 °C for 30 min and purged at the same temperature with helium gas (20 ml/min) to remove the physisorbed gas. The TPD run was then conducted from 100 to 700 °C at a heating rate of 5 °C/min.

### 2.3. Catalyst activity

The catalytic activity for vapor phase ODH of EB was investigated in a down flow fixed-bed stainless steel microreactor [36]. For each run, ~1.0 g of sample was loaded in the reactor. The reactor was heated to 600 °C at a rate of 2 °C/min in the flow of $N_2$ (20 ml/min) and kept at this temperature for 2 h and the $N_2$ was replaced with $CO_2$ gas. The catalyst pretreatment was continued at 600 °C for 30 min with $CO_2$ (20 ml/min) before conducting the reaction. The EB was introduced into the preheating zone of the reactor through a liquid feed pump with a constant feed rate of 9.8 mmol/h. Gaseous and liquid products were analyzed simultaneously by an on-line gas chromatograph (Younlin Instrument, Acme 6000 Series, Korea) equipped with TCD and FID. For analysis of liquid products, HP-innowax column (30 m long, 0.32 mm i.d. and 0.25 μm film thickness) was employed and for the gaseous products Porapak N 80/100 column (6 ft × 1/8 in.) was used. The main liquid products that were analyzed include styrene, benzene, toluene, benzaldehyde and acetophenone, and the gaseous products were hydrogen, methane, carbon monoxide and carbon dioxide.

**Table 1**
BET surface area and pore volume measurements of samples obtained in this study and calcined at 550 °C

| Sample | Composition (wt.%) | Surface area ($m^2\ g^{-1}$) | Pore volume ($ml\ g^{-1}$) |
|---|---|---|---|
| $TiO_2$–$ZrO_2$ | 1:1 (mole ratio) | 207 | 0.65 |
| $V_2O_5$/$TiO_2$–$ZrO_2$ | 15% $V_2O_5$ | 175 | 0.46 |
| $CeO_2$/$TiO_2$–$ZrO_2$ | 15% $CeO_2$ | 189 | 0.51 |
| $V_2O_5$–$CeO_2$/$TiO_2$–$ZrO_2$ | 7.5%$V_2O_5$ + 7.5%$CeO_2$ | 170 | 0.45 |

## 3. Results and discussion

The $N_2$ BET surface areas of various samples calcined at 550 °C are presented in Table 1. As can be noted from this table, the $TiO_2$–$ZrO_2$ mixed oxide synthesized by a coprecipitation method exhibited a high specific surface area of 207 $m^2\ g^{-1}$. Very interestingly, the $TiO_2$–$ZrO_2$ composite oxide displayed more specific surface area than its individual component oxides, $TiO_2$ (15 $m^2\ g^{-1}$) and $ZrO_2$ (25 $m^2\ g^{-1}$), respectively [36]. The high specific surface area of the titania–zirconia mixed oxide is due to porous nature of the oxides formed through the coprecipitation procedure adopted in this study [35]. A slight decrease in the specific surface area and pore volume could be noted in the case of vanadia and ceria impregnated samples (Table 1). The decrease in the specific surface area after impregnating with $V_2O_5$ or $CeO_2$ is mainly due to various factors such as penetration of the deposited active oxides into the pores of the support thereby narrowing its pore diameter and blocking some of the micropores, and solid-state reaction between the dispersed active oxide and the supporting oxides [38,39]. The XRD results described in the following paragraphs strongly support the latter possibility.

The XRD profiles of various samples calcined at 550 °C are shown in Fig. 1. As shown in Fig. 1, the $TiO_2$–$ZrO_2$ mixed oxide support is in an X-ray amorphous form. In particular, no independent diffraction lines due to crystalline $TiO_2$ (anatase or rutile) and $ZrO_2$ (monoclinic, tetragonal or cubic) phases were observed. Although it has been reported in the literature that tetragonal and monoclinic $ZrO_2$ and rutile $TiO_2$ could be formed at higher calcination temperatures in some cases, no such independent phases were noted in the present investigation [35]. This is mainly due to the use of different precursors and a different preparation method adopted in the present study. The XRD patterns of $V_2O_5$ and $CeO_2$ containing samples also revealed that the impregnated oxides are in a highly dispersed form over the amorphous $TiO_2$–$ZrO_2$ mixed oxide support or the crystallites formed are less than the detection capability of the XRD technique. The vanadia and ceria loadings selected in the present study are lower than the theoretical monolayer capacity of the $TiO_2$–$ZrO_2$ support, based on its specific surface area [38]. The necessary quantity of active oxide to cover the support surface as a two-dimensional monomolecular layer can be estimated from structural calculations [38]. For instance, from V–O bond lengths of crystalline $V_2O_5$, the monolayer surface coverage is estimated to be 0.145 wt.% $V_2O_5$ $m^{-2}$ of the support [38]. However, the monolayer coverage depends not only on the support surface area but also on the concentration of reactive surface hydroxyl groups apart from other preparative variables. It is also well known in the literature that for vanadia contents of less than monolayer coverage, the dispersed active component will be present as a two-dimensional vanadium oxide overlayer on the support surface [38,39]. Quantities more than monolayer coverage will have microcrystalline $V_2O_5$ particles in addition to the surface vanadium oxide overlayer. Thus, the XRD results are in agreement with earlier findings in the literature [35].

To establish the thermal stability of the catalysts, which is essential to understand their behavior for the ODH reaction at high temperatures, these samples were subjected to calcination at 750 °C. The XRD patterns of these samples are shown in Fig. 2. As shown in Fig. 2, the XRD patterns of $TiO_2$–$ZrO_2$ (SA = 112 $m^2\ g^{-1}$) sample revealed formation of a stable crystalline $ZrTiO_4$ compound [35]. The specific surface areas of all samples were decreased after calcination at 750 °C as expected due to the formation various nonporous crystalline compounds. No XRD patterns pertaining to any known or new crystalline compounds were noted in the case of $CeO_2$/$TiO_2$–$ZrO_2$ (SA = 96 $m^2\ g^{-1}$) sample except the same characteristic lines due to the $ZrTiO_4$ compound. This observation clearly indicates that the deposited ceria is in a highly dispersed form over the $TiO_2$–$ZrO_2$ support. In the case of $V_2O_5$/$TiO_2$–$ZrO_2$ (SA = 82 $m^2\ g^{-1}$) and $V_2O_5$–$CeO_2$/$TiO_2$–$ZrO_2$ (SA = 88 $m^2\ g^{-1}$) samples, some additional lines due to the formation of $ZrV_2O_7$ and $CeVO_4$ compounds, respectively were noted [35]. In the case of

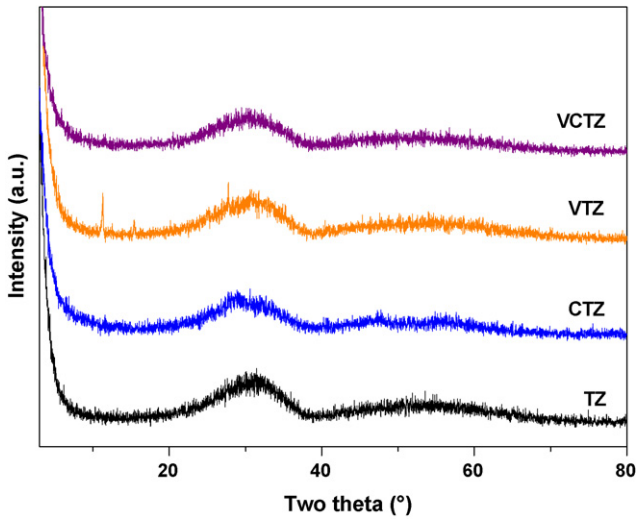


**Fig. 1.** X-ray powder diffractions of $TiO_2$–$ZrO_2$ (TZ), $CeO_2$/$TiO_2$–$ZrO_2$ (CTZ), $V_2O_5$/$TiO_2$–$ZrO_2$ (VTZ) and $V_2O_5$–$CeO_2$/$TiO_2$–$ZrO_2$ (VCTZ) samples calcined at 550 °C.

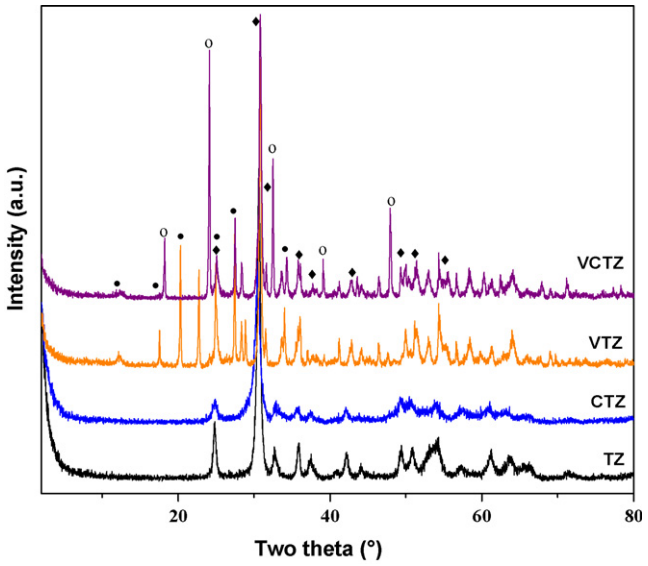


**Fig. 2.** X-ray powder diffractions of $TiO_2$–$ZrO_2$ (TZ), $CeO_2$/$TiO_2$–$ZrO_2$ (CTZ), $V_2O_5$/$TiO_2$–$ZrO_2$ (VTZ) and $V_2O_5$–$CeO_2$/$TiO_2$–$ZrO_2$ (VCTZ) samples calcined at 750 °C: (◆) lines due to $ZrTiO_4$, (●) lines due to $ZrV_2O_7$, (o) lines due to $CeVO_4$.

$TiO_2$–$ZrO_2$, formation of an amorphous phase at 550 °C and subsequent crystalline $ZrTiO_4$ compound at 750 °C calcination temperature could be due to a different preparation method adopted and the precursor compounds employed in the present study. This fact has also been documented in the literature [35]. The $TiO_2$–$ZrO_2$ mixed oxides tend to form highly stable $ZrTiO_4$ compound when using an appropriate preparation method and subjected to calcination temperatures beyond 550 °C. As revealed by XRD measurements (Figs. 1 and 2), the impregnated vanadium oxide is in a highly dispersed form over the amorphous titania–zirconia support after calcination at 550 °C and leads to better crystallization and formation of various compounds at 750 °C. A closer look into Figs. 1 and 2 also reveals that heating temperature and $V_2O_5$ have two primary effects on the $TiO_2$–$ZrO_2$ mixed oxide support: Transformation of amorphous $TiO_2$–$ZrO_2$ mixed oxide into a well-crystalline $ZrTiO_4$ compound and the appearance of $ZrV_2O_7$ lines. It is an established fact in the literature that highly dispersed vanadia on the titania surface accelerates the crystallization and transformation of $TiO_2$-anatase into rutile phase by lowering the activation temperature of this phenomenon [38,39]. During this transition, some of the dispersed vanadium oxide is incorporated into the rutile solid solution. A similar phenomenon is apparent in the case of vanadium oxide containing titania–zirconia mixed oxide samples.

The Raman spectra of various samples calcined at 550 °C are presented in Fig. 3. The spectrum of $TiO_2$–$ZrO_2$ mixed oxide calcined at 550 °C (Fig. 3a) contained broad bands at around 196, 306, 432, 738 and 980 $cm^{-1}$ that should be characteristic for an amorphous $ZrTiO_4$ compound. As per the literature, the Raman spectra of monoclinic and tetragonal $ZrO_2$ exhibit characteristic bands at around 103, 181, 190, 222, 310, 337, 382, 474, 499, 540, 559, 620, 636, 763 $cm^{-1}$ and a shoulder at 261–270, respectively [35,40]. On the other hand, the Raman spectrum of $TiO_2$-anatase exhibits bands at 144, 199, 399, 520 and 638, and the $TiO_2$-rutile phase at 144 and 611 $cm^{-1}$, respectively [41]. No characteristic bands pertaining to any of these individual component oxides were noted in the present study indicating their absence and the formation of an amorphous $ZrTiO_4$ compound, supporting the XRD results. The Raman spectrum of $TiO_2$–$ZrO_2$ sample calcined at 750 °C (Fig. 3e) exhibited several additional broad bands at around 196, 263, 337, 478, 635, 784 and 983 $cm^{-1}$, which could be assigned to the crystalline $ZrTiO_4$ compound whose presence has been established from XRD measurements [35]. Thus, the Raman results also establish the transformation of an amorphous titania–zirconia into a crystalline form at 750 °C calcination temperature [35]. In the case of $V_2O_5$/$TiO_2$–$ZrO_2$ sample, in addition to the broad background bands of $ZrTiO_4$ compound, a few extra broad bands were noted due to the dispersed vanadium oxide phase. According to the literature, the Raman bands of supported metal oxide catalysts in the range 1050–950 $cm^{-1}$ can be assigned to the stretching mode of the short terminal M=O bonds, whereas the bands in the range between 950 and 750 $cm^{-1}$ could be attributed to either the anti-symmetric stretch of the M–O–M bonds or the symmetric stretch of the (–O–M–O–)*n* bonds [42]. The major peak of crystalline $V_2O_5$ assigned to V=O stretching mode appears at around 995 $cm^{-1}$. Due to a relatively large Raman scattering cross-section of $V_2O_5$ as compared to the cross-section for supported vanadia species, Raman spectra of supported vanadia catalysts are essentially similar to the bulk $V_2O_5$ [42,43]. The bulk $V_2O_5$ exhibits characteristic bands at ~995, ~702, ~527, ~404, ~284 and ~146 $cm^{-1}$ [43]. In the case of $CeO_2$/$TiO_2$–$ZrO_2$ and $V_2O_5$–$CeO_2$/$TiO_2$–$ZrO_2$ samples, only the broad background bands due to an amorphous $ZrTiO_4$ compound could be noted. Pure $CeO_2$ exhibits an intense Raman band at 460 $cm^{-1}$ and smaller bands at 239 and 590 $cm^{-1}$, respectively [44]. Thus, the Raman measurements support some of the observations made from XRD study. In particular, these results support a high dispersion of the impregnated vanadium and cerium oxides over the titania–zirconia mixed oxide support.

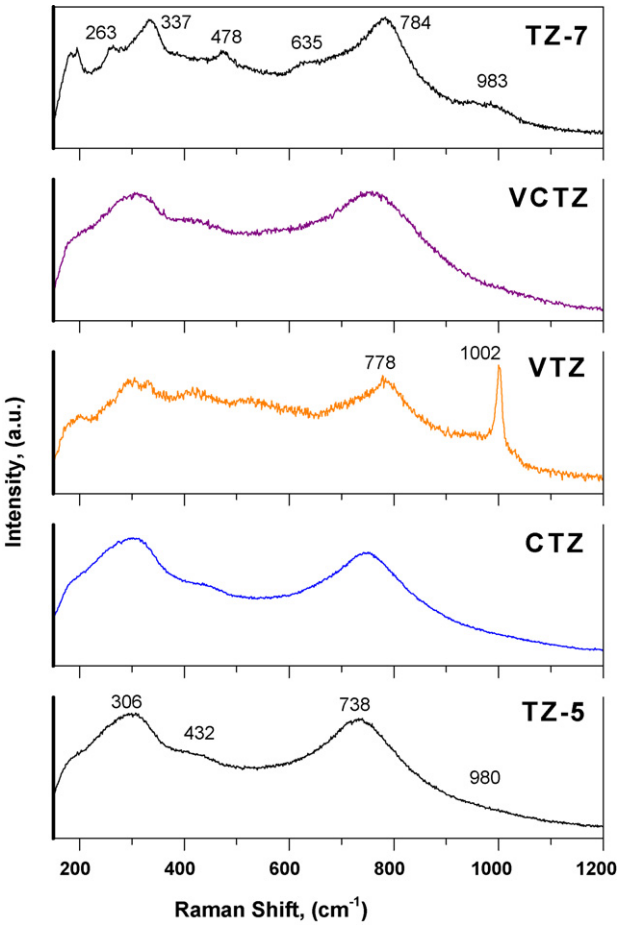


**Fig. 3.** Raman spectra of $TiO_2$–$ZrO_2$ (TZ-5), $CeO_2$/$TiO_2$–$ZrO_2$ (CTZ), $V_2O_5$/$TiO_2$–$ZrO_2$ (VTZ) and $V_2O_5$–$CeO_2$/$TiO_2$–$ZrO_2$ (VCTZ) samples calcined at 550 °C and $TiO_2$–$ZrO_2$ (TZ-7) sample calcined at 750 °C.

The external and internal morphologies of various samples calcined at 550 °C were examined by both SEM and TEM techniques, respectively. The representative SEM images of $TiO_2$–$ZrO_2$ and $V_2O_5$–$CeO_2$/$TiO_2$–$ZrO_2$ samples are shown in Fig. 4. The SEM images of all samples revealed typical spherical type agglomerates with varying sizes within the nanometer range. In particular, no big difference among various samples was noted from these images. However, the $TiO_2$–$ZrO_2$ support exhibited relatively good homogeneity with slightly sharp features. Interestingly, the addition of vanadium oxide to the $TiO_2$–$ZrO_2$ support resulted in a slight increase of the crystallite sizes. On the other hand, the addition of cerium oxide to $TiO_2$–$ZrO_2$ showed an opposite effect. The combined influence of $V_2O_5$ and $CeO_2$ were reflected in the SEM images of the $V_2O_5$–$CeO_2$/$TiO_2$–$ZrO_2$ sample. The TEM results, as shown in Fig. 5, also supported the information obtained from other techniques. The $TiO_2$–$ZrO_2$ support is composed of snowflake type networks with nanometer-sized particles (Fig. 5a). This morphology generally leads to a loose structure with high specific surface area and pore volume, which have been confirmed by $N_2$ adsorption measurements. The addition of vanadium and cerium oxides had some strong influence on the morphology of the $TiO_2$–$ZrO_2$ support as revealed by the TEM images. Here again, the TEM images of $V_2O_5$–$CeO_2$/$TiO_2$–$ZrO_2$ sample revealed combined

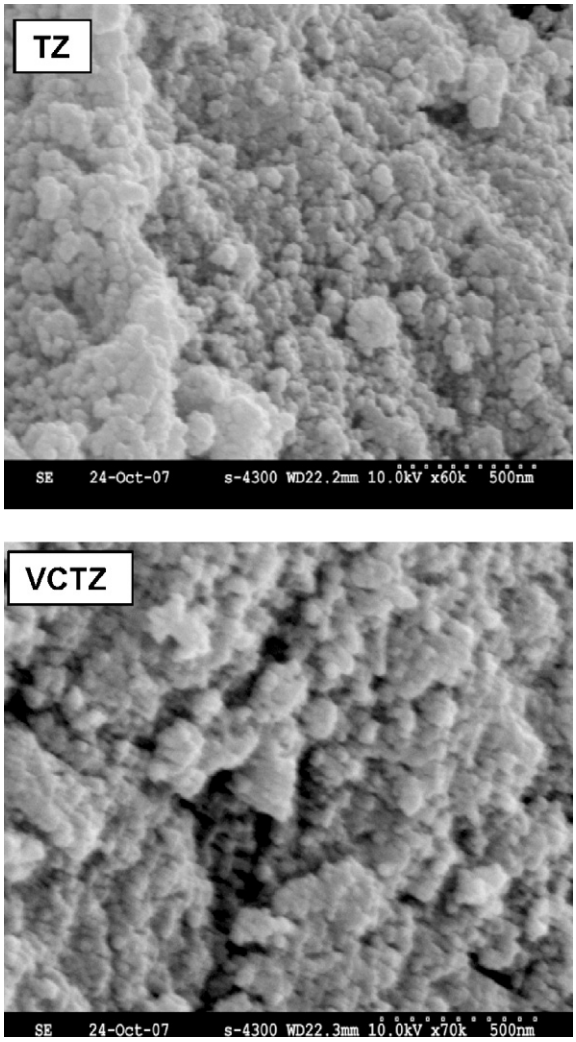


**Fig. 4.** SEM images of $TiO_2$–$ZrO_2$ (TZ) and $V_2O_5$–$CeO_2$/$TiO_2$–$ZrO_2$ (VCTZ) samples calcined at 550 °C.

features of $V_2O_5$/$TiO_2$–$ZrO_2$ and $CeO_2$/$TiO_2$–$ZrO_2$ samples, respectively. In particular, $V_2O_5$/$TiO_2$–$ZrO_2$ and $V_2O_5$–$CeO_2$/$TiO_2$–$ZrO_2$ samples revealed clearly having ~8–10 nm sized grains and the other samples are slightly blow this size. As mentioned earlier, better crystallization is due to the influence of vanadium oxide, which is known to accelerate the crystallization of titania and zirconia phases [35].

Temperature programmed reduction profiles of various samples calcined at 550 °C are shown in Fig. 6. The TPR profiles revealed some interesting information about the relative reducibly of these mixed oxides. The TPR peaks were not well resolved under the experimental conditions employed in this study. Therefore, quantification of the data was not attempted. The $TiO_2$–$ZrO_2$ support exhibited a sharp reduction peak at ~748 °C and another broad and continuous peak at around 870 °C. The TPR results revealed that $TiO_2$–$ZrO_2$ mixed oxide is quite stable which is primarily due to the formation of an amorphous or crystalline $ZrTiO_4$ compound inline with literature reports [35,36]. As per the literature, the bulk $V_2O_5$ exhibits multiple reduction peaks, which are due to the reduction sequence of $V_2O_5 \rightarrow V_6O_{13}$ (~853 °C), $V_6O_{13} \rightarrow V_2O_4$ (~1004 °C) and $V_2O_4 \rightarrow V_2O_3$ (~1008 °C), respectively [45]. Interestingly, the $V_2O_5$/$TiO_2$–$ZrO_2$ catalyst also exhibited a similar TPR profile of the bulk $V_2O_5$. However, the reduction temperatures of all the peaks were decreased due to the influence of the $TiO_2$–$ZrO_2$ support. Normally, the crystallites size combined with crystal orientation play a major role in the reduction behavior of various oxides. As envisaged in the literature, the unsupported $V_2O_5$ has a random orientation of various crystallographic planes exposed to the reduction gas mixture, whereas the supported $V_2O_5$ displays a preferred orientation and exhibits better reducibility [45]. Accordingly, the dispersed vanadia over the $TiO_2$–$ZrO_2$ support is expected to reduce at a lower temperature than the bulk $V_2O_5$. Reduction of bulk $CeO_2$ is facile and known to reduce at lower temperatures [46]. Bulk ceria also exhibits at least three reduction peaks due to the removal of adsorbed oxygen on the surface as well as surface and bulk reduction of $CeO_2 \rightarrow Ce_2O_3$. The last two peaks are normally observed at higher temperatures with about 250 °C difference in their peak maxima temperatures [46]. Similar to $V_2O_5$/$TiO_2$–$ZrO_2$ sample, the reduction temperature of $CeO_2$/$TiO_2$–$ZrO_2$ has also been shifted to lower temperatures (~485 and 607 °C). The $V_2O_5$–$CeO_2$/$TiO_2$–$ZrO_2$ sample exhibited a broad and well-defined reduction peak at 598 °C and another weak and broad peak at 780 °C. This profile is different from the reduction profiles of $V_2O_5$/$TiO_2$–$ZrO_2$ and $CeO_2$/$TiO_2$–$ZrO_2$ samples, respectively. The intense peak is primarily due to the reduction of the dispersed ceria–vanadia mixed oxide phase over the titania–zirconia support, which is formed owing to solid-state reactions between them. This peculiar reduction phenomenon has been reflected in its high and very stable catalytic activity, which is being dealt in the later paragraphs.

To understand the acid–base properties of these oxides, temperature programmed desorption of $CO_2$ was undertaken. In general, TPD measurements provide meaningful information about the available adsorption sites as well as the way in which the key species are chemisorbed on the catalyst surface. It is well known that the acidity and basicity of the catalysts are often related to the catalytic activity in many acid–base catalyzed reactions [30]. The $CO_2$ is known to be an acidic gas; its adsorption on the catalyst surface is strongly affected by the basic property of the solids [36]. It can be assumed from the literature that one $CO_2$ molecule adsorbs on one basic site of the catalyst. If the distribution of basic sites on the catalyst surface is uniform then it can be related to the number of basic sites of the catalysts [36]. On the other hand, desorption temperature maximum ($T_{max}$) is a characteristic of the basic strength. As shown in Fig. 7, the TPD profiles of all samples revealed relatively broad desorption peaks with different peak maxima reflecting their acid–base properties. In view of very board nature of the peaks, quantification of the peaks was not attempted. The signal intensities were also not normalized to make quantitative comparison. The $CO_2$ TPD profile of $TiO_2$–$ZrO_2$ sample revealed that the strength and number of basic sites are higher than that of its individual component oxides [36]. Interestingly, the TPD profile of $V_2O_5$–$CeO_2$/$TiO_2$–$ZrO_2$ sample also revealed very broad peaks and reflected the combination of both $V_2O_5$–$CeO_2$/$TiO_2$–$ZrO_2$ and $V_2O_5$–$CeO_2$/$TiO_2$–$ZrO_2$ profiles. Indeed, the same characteristic property is reflected in its catalytic behavior. The TPD and TPR studies provide good evidence that the $V_2O_5$–$CeO_2$/$TiO_2$–$ZrO_2$ sample exhibits different characteristic properties than its independent $V_2O_5$/$TiO_2$–$ZrO_2$ and $CeO_2$/$TiO_2$–$ZrO_2$ samples, thus signifying the influence of ceria incorporation into this catalyst system.

The catalytic activity and selectivity results for EB to styrene employing $CO_2$ as the oxidant over various samples calcined at 550 °C and evaluated at 600 °C are presented in Fig. 8. In general, the conversion of EB increased with increasing reaction temperature from 500 °C and all catalysts followed a similar trend. However, for better comparison among various catalysts and with previously reported catalysts, the catalytic activity data were

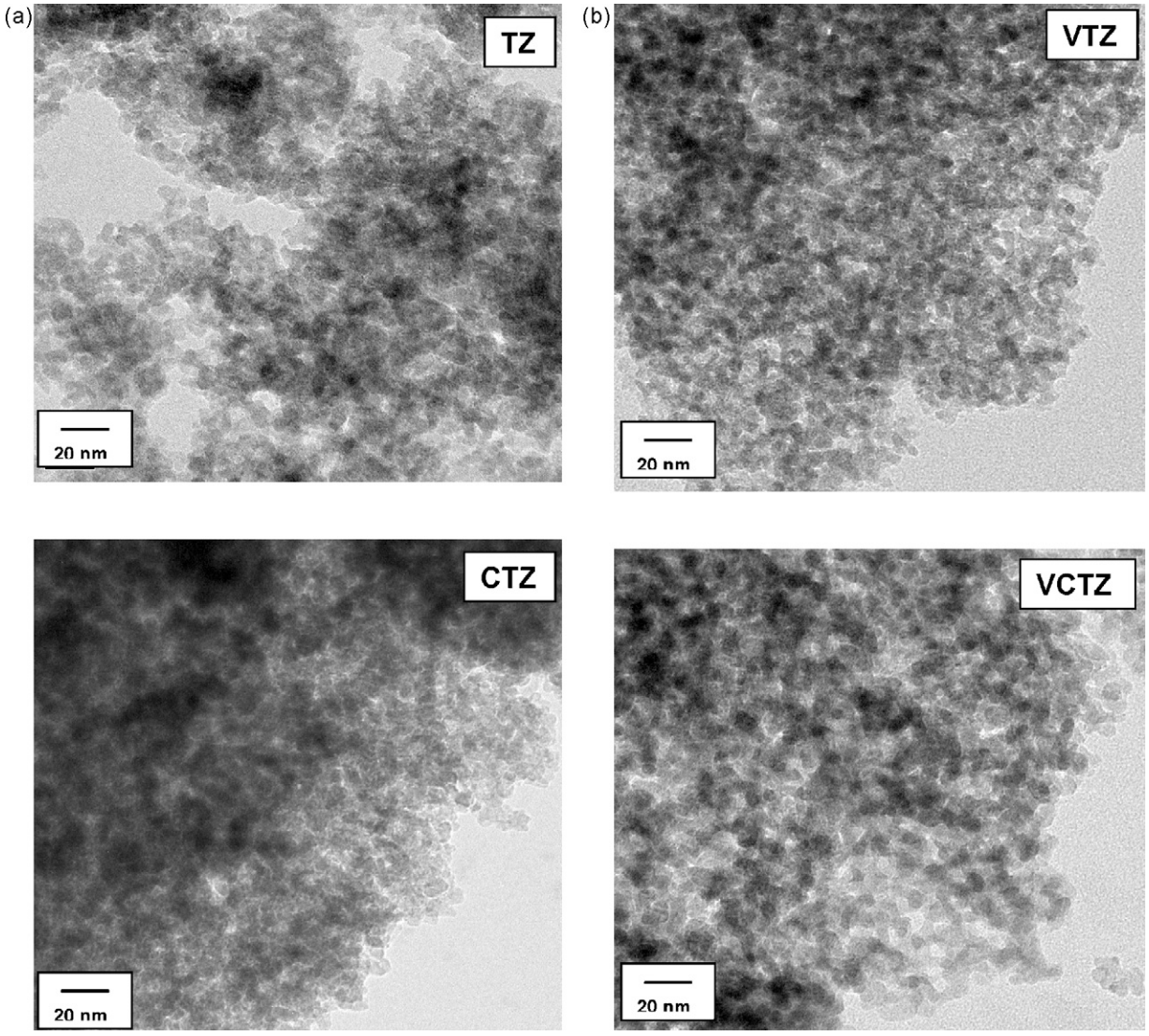


**Fig. 5.** TEM images of $TiO_2$–$ZrO_2$ (TZ), $CeO_2/TiO_2$–$ZrO_2$ (CTZ), $V_2O_5/TiO_2$–$ZrO_2$ (VTZ) and $V_2O_5$–$CeO_2/TiO_2$–$ZrO_2$ (VCTZ) samples calcined at 550 °C.

generated at a constant temperature and optimum space velocity. Further, the activity of the catalysts (except $V_2O_5/TiO_2$–$ZrO_2$) was found to improve with time in the first few hours of the reaction. Therefore, for comparison the catalytic data obtained after 3–4 h has been considered. All promoted samples exhibited better conversion than that of the $TiO_2$–$ZrO_2$ support. In addition, the $V_2O_5$–$CeO_2/TiO_2$–$ZrO_2$ combination catalyst exhibited better conversion and product selectivity than all other samples. Our earlier study revealed that $TiO_2$–$ZrO_2$ mixed oxide exhibits exceptionally better conversion and product selectivity than its individual component oxides ($TiO_2$ and $ZrO_2$) under identical reaction conditions [36]. The observed high activity and selectivity of the $TiO_2$–$ZrO_2$ was proved to be due to the formation of an amorphous mixed oxide phase, enhancement in the specific surface area, and an increase in the number and strength of acid–base sites [6,36]. In particular, the origin of $TiO_2$–$ZrO_2$ mixed oxide also plays a major role in its catalytic behavior [36]. Most importantly, the presence of anion impurities alters the acid–base properties of these oxides, which in turn influence their catalytic behavior. In the present investigation, the $TiO_2$–$ZrO_2$ mixed oxide was synthesized without anion impurities, which resulted in high specific surface area, however less active than earlier preparation [36].

A fast catalyst deactivation is often encountered on most of the catalyst systems in the dehydrogenation of EB to styrene. Therefore, time-on-stream measurements are most significant to understand the behavior of various catalyst systems. As shown in Fig. 9, the time-on-stream experiments revealed interesting information about the catalytic behavior of these systems toward the ODH of EB. The $V_2O_5$–$CeO_2/TiO_2$–$ZrO_2$ sample exhibited relatively stable activity and selectivity in the time-on-stream experiments. Interestingly, the $V_2O_5/TiO_2$–$ZrO_2$ sample exhibited a high conversion in the first few hours of the reaction. However, a fast decrease in the conversion was noted due to deactivation of the catalyst owing to coke formation as confirmed by an increase in the weight of the sample after the catalytic experiment. On the other hand, the $CeO_2/TiO_2$–$ZrO_2$ sample showed relatively stable activity, however less conversion. The activity results thus revealed a good catalytic efficiency of $V_2O_5$–$CeO_2$ combination, which exhibited stable activity without rapid deactivation. To obtain some information about the deactivation phenomenon of these catalysts, the spent catalysts were subjected to XRD analysis. The XRD patterns of the used samples are shown in Fig. 10. Except $V_2O_5/TiO_2$–$ZrO_2$ catalyst, all other samples exhibited an amorphous nature similar to that of the fresh catalysts. In the case of $V_2O_5/TiO_2$–$ZrO_2$ catalyst, XRD lines due to the formation

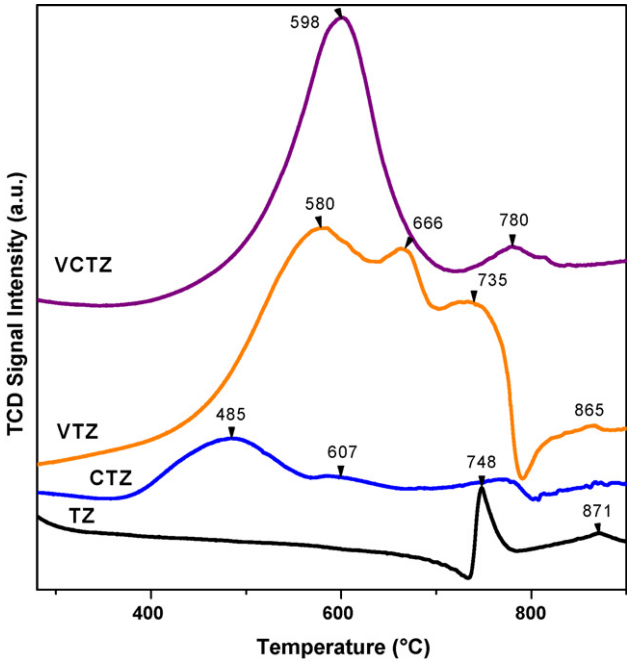


**Fig. 6.** The TPR ($H_2$) profiles of $TiO_2$–$ZrO_2$ (TZ), $CeO_2$/$TiO_2$–$ZrO_2$ (CTZ), $V_2O_5$/$TiO_2$–$ZrO_2$ (VTZ) and $V_2O_5$–$CeO_2$/$TiO_2$–$ZrO_2$ (VCTZ) samples calcined at 550 °C. The peak intensities are not normalized.

crystalline $ZrTiO_4$ compound were noted. After the catalytic experiment, no apparent change of color and increase in the weight of the sample were noted in the case of $CeO_2$/$TiO_2$–$ZrO_2$ and $V_2O_5$–$CeO_2$/$TiO_2$–$ZrO_2$ samples indicating no coke formation over the surface of these catalysts. This observation clearly signifies the role of ceria in preventing the catalyst deactivation and keeping a high and stable catalytic activity. Recent literature reports also reveal that ceria and ceria–zirconia mixed oxides produce stable catalytic activity during time-on-stream runs in different reactions. $NiO_x$/$CeO_2$–$ZrO_2$ combination catalyst exhibited a stable activity for syngas production via $CO_2$ reforming of methane without significant loss [25]. Similar observations were reported for partial oxidation of methane (POM) [47] and dehydration of 4-methyl-2-pentanol [48]. On the contrary, a rapid deactivation was noted in the case of $VO_x$/$Al_2O_3$ catalyst [10]. The stable activity of various catalysts is mainly due to facile oxygen transport from the bulk of $CeO_2$ or $Ce_xZr_{1-x}O_2$ solid solutions that help in the prevention of coke formation, which is the main deactivation pathway of these catalysts. Thus, the observed stable activity for the ODH of EB in the present study is in good agreement with literature reports. The remarkable ability of $CeO_2$ in $V_2O_5$/$TiO_2$–$ZrO_2$ catalysts to maintain a high and stable activity is clearly apparent from the present study.

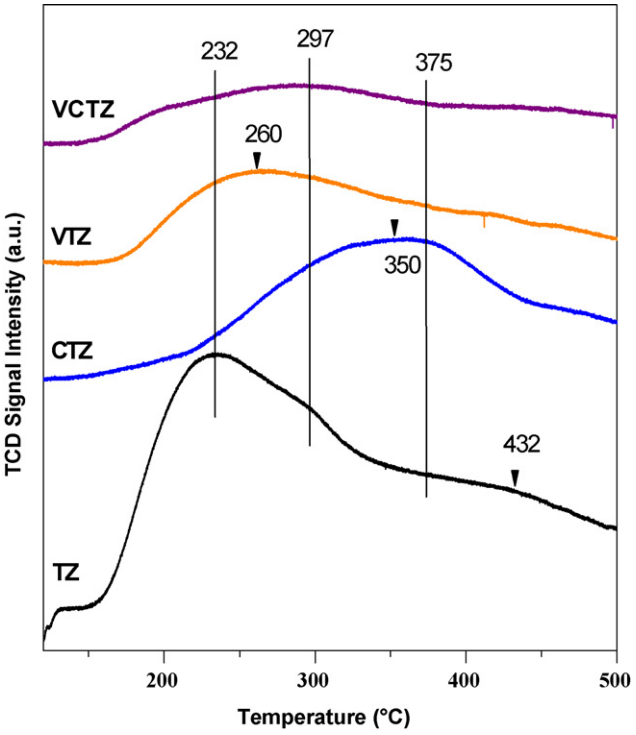


**Fig. 7.** The TPD ($CO_2$) profiles of $TiO_2$–$ZrO_2$ (TZ), $CeO_2$/$TiO_2$–$ZrO_2$ (CTZ), $V_2O_5$/$TiO_2$–$ZrO_2$ (VTZ) and $V_2O_5$–$CeO_2$/$TiO_2$–$ZrO_2$ (VCTZ) samples calcined at 550 °C. The peak intensities are not normalized.

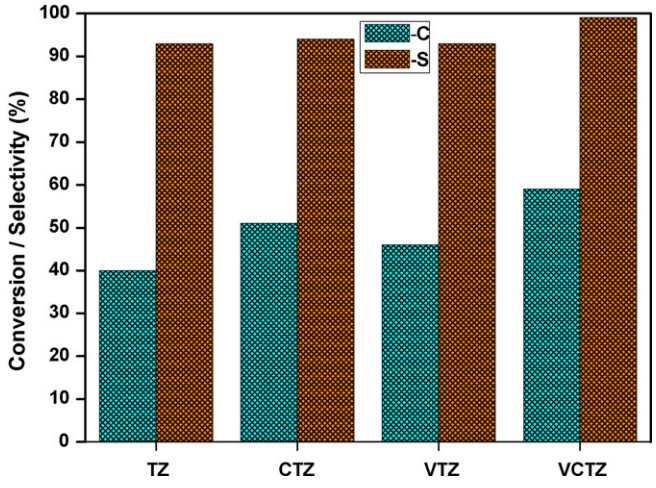


**Fig. 8.** Ethylbenzene conversion (C) styrene selectivity (S), on $TiO_2$–$ZrO_2$ (TZ), $CeO_2$/$TiO_2$–$ZrO_2$ (CTZ), $V_2O_5$/$TiO_2$–$ZrO_2$ (VTZ) and $V_2O_5$–$CeO_2$/$TiO_2$–$ZrO_2$ (VCTZ) samples calcined at 550 °C. Reaction conditions: $T$ = 600 °C, $P$ = 1 atm., W/F = 16.73 g cat, h/mole, $CO_2$/EB = 5.1 (molar ratio).

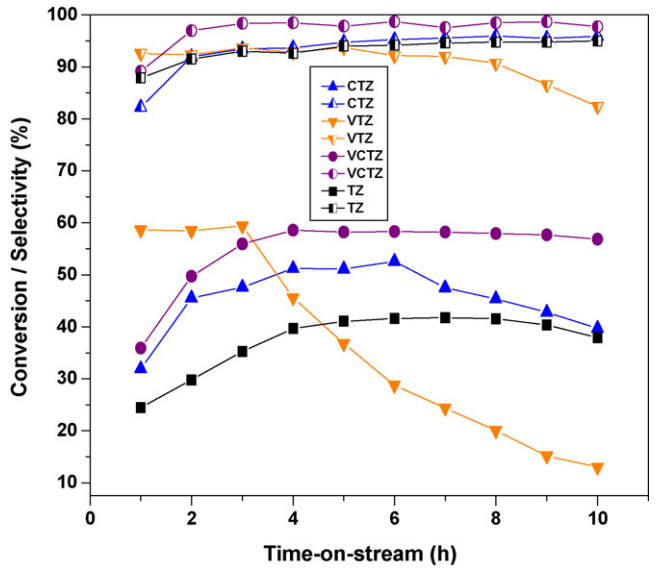


**Fig. 9.** Variation of catalytic activity and selectivity with time-on-stream over $TiO_2$–$ZrO_2$ (TZ), $CeO_2$/$TiO_2$–$ZrO_2$ (CTZ), $V_2O_5$/$TiO_2$–$ZrO_2$ (VTZ) and $V_2O_5$–$CeO_2$/$TiO_2$–$ZrO_2$ (VCTZ) samples calcined at 550 °C. Reaction conditions: $T$ = 600 °C, $P$ = 1 atm., W/F = 16.73 g cat, h/mole, $CO_2$/EB = 5.1 (molar ratio).

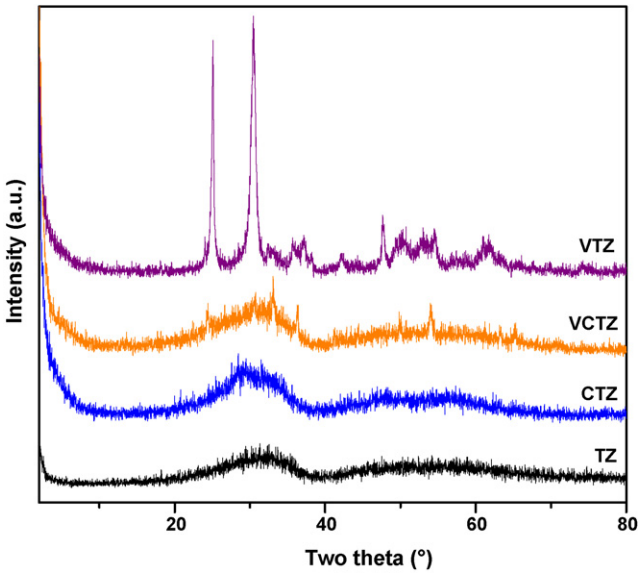


**Fig. 10.** X-ray powder diffractions of used $TiO_2$–$ZrO_2$ (TZ), $CeO_2$/$TiO_2$–$ZrO_2$ (CTZ), $V_2O_5$/$TiO_2$–$ZrO_2$ (VTZ) and $V_2O_5$–$CeO_2$/$TiO_2$–$ZrO_2$ (VCTZ) catalyst samples after catalytic activity measurements.

To investigate the potential role of $CO_2$ in directing the product formation and catalyst stability, we have investigated a $TiO_2$–$ZrO_2$ sample for its activity and selectivity during time-on-stream measurements in the presence and absence of $CO_2$ [36]. As noticed in the present study, the conversion of EB and selectivity of styrene were slightly lower in the first 2–3 h of the reaction. From third hour onwards an enhancement in the activity was noticed. However, a significant difference in the EB conversion, styrene selectivity, and catalyst stability were noted between $CO_2$ and $N_2$ feed gases, suggesting that a simple dehydrogenation of EB is taking place without $CO_2$ (Eq. (1)); whereas in the presence of $CO_2$ the reverse water-gas-shift (RWGS) reaction (Eq. (2)) coupled with the simple dehydrogenation are taking place as shown in Eqs. (1) and (2) [36].

$$C_6H_5CH_2{-}CH_3 \rightarrow C_6H_5CH = CH_2 + H_2 (\text{dehydrogenation}) \quad (1)$$

$$H_2 + CO_2 \rightarrow CO + H_2O\,(\text{RWGS}) \quad (2)$$

As envisaged by Cavani and Trifiro [6], the oxidation of hydrogen by $CO_2$ shifts the dehydrogenation equilibrium to achieve higher yields by increasing the conversion as well as selectivity. In a recent study, Sun et al. [49] also explained the role of $CO_2$ by coupling the RWGS reaction with the EB dehydrogenation. In addition, several studies emphasized the mechanism of ODH of EB to styrene in the presence of $CO_2$ in which redox sites operate either with the single step pathway (Eq. (3)) or the dual step pathway (Eqs. (3) and (4)) [16,21,26,49]. More details on these mechanisms could be found elsewhere [2,5,6].

$$C_6H_5CH_2{-}CH_3 + CO_2 \rightarrow C_6H_5CH = CH_2 + H_2O \quad (3)$$

$$C_6H_5CH_2{-}CH_3 \rightarrow C_6H_5CH = CH_2 + H_2 \quad (4)$$

The catalytic activity and selectivity results from the present study reveal that vanadia and ceria impregnated titania–zirconia mixed oxides exhibit a stable catalytic activity with high conversion and product selectivity in the ODH of EB to styrene with $CO_2$ as the soft oxidant.

## 4. Conclusions

The following conclusions can be drawn from this investigation: (1) The $TiO_2$–$ZrO_2$ mixed oxide obtained by a coprecipitation method exhibits a high specific surface area and X-ray amorphous when calcined at 550 °C. The amorphous titania–zirconia has been converted into a crystalline $ZrTiO_4$ compound when calcined at 750 °C. (2) The $TiO_2$–$ZrO_2$ composite oxide is an interesting carrier for the dispersion of vanadium and cerium oxides. As revealed by XRD and RS techniques, the deposited vanadium and cerium oxides are in a highly dispersed form over the $TiO_2$–$ZrO_2$ support when calcined at 550 °C. The SEM and TEM studies revealed that the dispersed vanadium oxide strongly interacts with cerium oxide on the $TiO_2$–$ZrO_2$ carrier. The XRD studies further indicate the formation of crystalline $ZrV_2O_7$ and $CeVO_4$ in addition to the $ZrTiO_4$ when these samples were subjected to 750 °C. In particular, the dispersed vanadium oxide accelerates this crystallization process. (3) The TPR and TPD studies revealed that the reduction and desorption profiles, respectively of the $V_2O_5$–$CeO_2$/$TiO_2$–$ZrO_2$ sample are exact replication of the profiles of $V_2O_5$/$TiO_2$–$ZrO_2$ and $CeO_2$/$TiO_2$–$ZrO_2$ samples and indicate the significance of addition. (4) The $TiO_2$–$ZrO_2$ mixed oxide and its promoted analogues exhibit good catalytic activity and selectivity for the ODH of EB with $CO_2$ as an oxidant. In particular, the $V_2O_5$–$CeO_2$/$TiO_2$–$ZrO_2$ combination catalyst exhibits relatively high and stable activity in the time-on-stream experiments. Undoubtedly, the remarkable ability of $CeO_2$ in $V_2O_5$/$TiO_2$–$ZrO_2$ catalysts to obtain a high and stable activity has been clearly established from the present study.

## Acknowledgments

This work was supported by Korea Science and Engineering Foundation (KOSEF) grant founded by the Korea Government (MEST) (NRL NO. 36379-1). BMR thanks Korea Federation of Science and Technology (KOFST) for a visiting fellowship under Brain Pool program.

## References

[1] S.-E. Park, J.-S. Chang, K.-W. Lee (Eds.), Study Surf. Sci. Catal., vol. 153, Elsevier, Amsterdam, 2004, p. xiii.
[2] S.-E. Park, S.-C. Han, J. Ind. Eng. Chem. 7 (2004) 1257–1269.
[3] J.-S. Chang, D.-Y. Hong, V.P. Vislovskiy, S.-E. Park, Catal. Surv. Asia 11 (2007) 59–69.
[4] B.M. Reddy, D.-S. Han, N. Jiang, S.-E. Park, Catal. Surv. Asia 12 (2008) 56–69.
[5] E.H. Lee, Catal. Rev. Sci. Eng. 8 (1974) 285–305.
[6] F. Cavani, F. Trifiro, Appl. Catal. A: Gen. 133 (1995) 219–239.
[7] K. Kochloefl, in: G. Ertl, H. Knözinger, J. Weitkamp (Eds.), Handbook of Heterogeneous Catalysis, vol. 5, VCH, Weinhein, 1998, p. 2151.
[8] N. Mimura, I. Takahara, M. Saito, T. Hattori, K. Ohkuma, M. Ando, Catal. Today 45 (1998) 61–64.
[9] M.M. Bhasin, J.H. McCain, B.V. Vora, T. Imai, P.R. Pujado, Appl. Catal. A: Gen. 221 (2001) 397–419.
[10] N.R. Shiju, M. Anilkumar, S.P. Mirajkar, C.S. Gopinath, B.S. Rao, C.V.V. Satyanarayana, J. Catal. 230 (2005) 484–492.
[11] B.M. Reddy, K.N. Rao, G.K. Reddy, A. Khan, S.-E. Park, J. Phys. Chem. C 111 (2007) 18751–18758.
[12] W.S. Chang, Y.Z. Chen, B.L. Yang, Appl. Catal. A: Gen. 124 (1995) 221–229.
[13] C.R. Adams, T.J. Jennings, J. Catal. 17 (1970) 157–177.
[14] H. Sun, H. Wang, J. Zhang, Appl. Catal. B: Environ. 73 (2007) 158–165.
[15] M. Rezaei, S.M. Alavi, S. Sahebdelfar, P. Bai, X. Liu, Z.-F. Yan, Appl. Catal. B: Environ. 77 (2008) 346–354.
[16] M. Sugino, H. Shimada, T. Turuda, H. Miura, N. Ikenaga, T. Suzuki, Appl. Catal. A: Gen. 121 (1995) 125–137.
[17] J.S. Yoo, Catal. Today 41 (1998) 409–410.
[18] R. Dziembaj, P. Kustrowski, T. Badstube, H. Papp, Top. Catal. 11/12 (2000) 317–326.
[19] S. Chen, Z. Qin, A. Sun, J. Wang, J. Nat. Gas Chem. 15 (2006) 11–14.
[20] N. Mimura, I. Takahara, M. Saito, Y. Sasaki, K. Murata, Catal. Lett. 78 (2002) 125.
[21] Y. Sakurai, T. Suzaki, K. Nakagawa, N. Ikenaga, H. Aota, T. Suzuki, J. Catal. 209 (2002) 16–24.

[22] M. Saito, H. Kimura, N. Mimura, J. Wu, K. Murata, Appl. Catal. A: Gen. 239 (2003) 71–77.
[23] G. Carja, R. Nakamura, T. Aida, H. Niiyama, J. Catal. 218 (2003) 104–110.
[24] S.-E. Park, J.-S. Chang, J.S. Yoo, in: M.M. Maroto-Valer, Y. Soong, C. Song (Eds.), Environmental Challenges and Greenhouse Gas Control for Fossil Fuel Utilization in the 21st Century, Kluwer Academic/Plenum Publishers, New York, 2002 p. 359.
[25] M.-S. Park, V.P. Vislovskiy, J.-S. Chang, Y.-G. Shul, J.S. Yoo, S.-E. Park, Catal. Today 87 (2003) 205–212.
[26] J.-S. Chang, V.P. Vislovskiy, M.-S. Park, D.-Y. Hong, J.S. Yoo, S.-E. Park, Green Chem. 5 (2003) 205–208.
[27] D.-Y. Hong, J.-S. Chang, J.-H. Lee, V.P. Vislovskiy, S.H. Jhung, S.-E. Park, Y.-H. Park, Catal. Today 112 (2006) 86–88.
[28] K. Chen, A. Khodakov, J. Yang, A.T. Bell, E. Iglesia, J. Catal. 186 (1999) 325.
[29] H.H. Kung, Adv. Catal. 40 (1994) 1–41.
[30] B.M. Reddy, in: J.L.G. Fierro (Ed.), Metal Oxides: Chemistry and Applications, Taylor & Francis, 2006, p. 215, Chapter 8.
[31] A. Trovarelli, Catalysis by Ceria and Related Materials; Catalytic Science Series 2, World Scientific Publishing Company, London, UK, 2002, p. 1.
[32] W. Daniell, A. Ponchel, S. Kuba, F. Anderle, T. Weingand, D.H. Gregory, H. Knözinger, Top. Catal. 20 (2002) 65–74.
[33] T. Feng, J.M. Vohs, J. Catal. 221 (2004) 619–629.
[34] S.T. Oyama, G.T. Went, K.B. Lewis, A.T. Bell, G.A. Somorjai, J. Phys. Chem. 93 (1989) 6786–6790.
[35] B.M. Reddy, A. Khan, Catal. Rev. Sci. Eng. 47 (2005) 257–296 (references therein).
[36] D.R. Burri, K.-M. Choi, S.-C. Han, A. Burri, S.-E. Park, Bull. Korean Chem. Soc. 28 (2007) 53–58 (references therein).
[37] D.R. Burri, K.-M. Choi, S.-C. Han, A. Burri, S.-E. Park, J. Mol. Catal. A: Chem. 269 (2007) 58–63.
[38] G.C. Bond, S.F. Tahir, Appl. Catal. 71 (1991) 1–17.
[39] B.M. Reddy, P. Lakshmanan, A. Khan, J. Phys. Chem. B 108 (2004) 16855–16863.
[40] M. Kilo, Ch. Schild, A. Wokaun, A. Baiker, J. Chem. Soc. Faraday Trans. 88 (1992) 1453–1462.
[41] I.R. Beattie, T.R. Gilson, J. Chem. Soc. A (1969) 2322–2328.
[42] H. Eckert, I.E. Wach, J. Phys. Chem. 93 (1989) 6796–6805.
[43] J.-M. Jehng, J. Phys. Chem. B 102 (1998) 5816–5822.
[44] B.M. Reddy, A. Khan, Y. Yamada, T. Kobayashi, M. Aouine, S. Loridant, J.C. Volta, J. Phys. Chem. B 109 (2005) 3355–3363.
[45] M.M. Koranne, J.G. Goodwin Jr., G. Marcelin, J. Catal. 148 (1994) 388–391.
[46] C. Decarne, E. Abi-Aad, B.G. Kostyuk, V.V. Lunin, A. Aboukais, J. Mater. Sci. 39 (2004) 2349–2356.
[47] M. Chen, H. Zheng, C. Shi, R. Zhou, X. Zheng, J. Mol. Catal. A: Chem. 237 (2005) 132–141.
[48] B.M. Reddy, P. Lakshmanan, P. Bharali, P. Saikia, J. Mol. Catal. A: Chem. 258 (2006) 355–360.
[49] A. Sun, Z. Qin, S. Chen, J. Wang, J. Mol. Catal. A: Chem. 210 (2004) 189–195.